Biosensors and Bioelectronics 90 (2017) 321–328

Contents lists available at ScienceDirect

Biosensors and Bioelectronics

journal homepage: www.elsevier.com/locate/bios

Construction of iron-polymer-graphene nanocomposites with low nonspecific adsorption and strong quenching ability for competitive immunofluorescent detection of biomarkers in GM crops

Kaifei Yin[1], Anran Liu[1,*], Li Shangguan, Li Mi, Xu Liu, Yuanjian Liu, Yuewu Zhao, Ying Li, Wei Wei, Yuanjian Zhang, Songqin Liu

Jiangsu Engineering Laboratory of Smart Carbon-Rich Materials and Device (CMD), Jiangsu Province Hi-Tech Key Laboratory for Bio-medical Research, School of Chemistry and Chemical Engineering, Southeast University, Nanjing 211189, PR China

ARTICLE INFO

Keywords:
Graphene
Protein
Fluorescence
Immunoassay
Biosensors

ABSTRACT

We developed a new immunofluorescent biosensor by utilizing a novel nanobody (Nb) and iron-polymer-graphene nanocomposites for sensitive detection of 5-enolpyruvylshikimate-3-phosphate synthase from Agrobacdterium tumefaciens strain CP4 (CP4-EPSPS), which considered as biomarkers of genetically modified (GM) crops. Specifically, we prepared iron doped polyacrylic hydrazide modified reduced graphene nanocomposites (Fe@RGO/PAH) by in-situ polymerization approach and subsequent a one-pot reaction with hydrazine. The resulting Fe@RGO/PAH nanocomposites displayed low nonspecific adsorption to analytes (11% quenching caused by nonspecific adsorption) due to electrostatic, energetic and steric effect of the nanocomposites. After Nb immobilizing, the as-prepared Fe@RGO/PAH/Nbs showed good selectivity and high quenching ability (92% quenching) in the presence of antigen (Ag) and polyethylene glycol (PEG) modified CdTe QDs (Ag/QDs@PEG), which is a nearly 4 fold than that of the unmodified GO in same condition. The high quenching ability of Fe@RGO/PAH/Nbs can be used for detection of CP4-EPSPS based on competitive immunoassay with a linearly proportional concentration range of 5–100 ng/mL and a detection limit of 0.34 ng/mL. The good stability, reproducibility and specificity of the resulting immunofluorescent biosensor are demonstrated and might open a new window for investigation of fluorescent sensing with numerous multifunctional graphene based materials.

1. Introduction

In the past decades, the use of genetically modified organisms (GMO) has been a topic of extensive discussion and contradictory opinions. Up to 2013, the area of biotech crops totalizing 175.2 million hectares, and exceed 79% were transgenic soybean, cotton and corn (Singh et al., 2015.). Because of the food safety and environmental safety issues accompanied with GMO, the detection of GMO in agriculture has generated considerable interest. The vast majority of these GM crops contain a gene named 5-enolpyruvylshikimate-3-phosphate synthase (EPSPS) from Agrobacterium tumefaciens strain CP4 (Chang et al., 2014), which is reported resistant to herbicide glyphosate (N-phosphonomethylglycine) (Swope et al., 2015). So far, the CP4-EPSPS is widespread in GM crops and can be regard as a potential marker for GM crops screening (Marani et al., 2015). Although the current testing method such as Enzyme–linked immunosorbent assay (ELISA) (Ahmed, 2002), Real time PCR techniques (Lerat et al., 2007) and Liquid chromatography tandem mass spectrometry (LC–MS/MS) (Ocana et al., 2009) are also explored to determination of CP4-EPSPS, they are suffering significantly from limited sensitivity and sophisticated equipment or involve tedious and painstaking procedures. Therefore, the ultrasensitive and low-cost technique for accurate detection of CP4-EPSPS is still of critical urgency.

Graphene based fluorescent detection has been widely used in many biosensors. Among these sensors, graphene oxide (GO) were commonly combined with organic fluorophores for fluorescent detection (Chang et al., 2010; Lu et al., 2009; Zhang et al., 2011a, 2011b) and GO served as both quencher of fluorophores and carrier of biomolecule probes. Comparing with the traditional quenchers like gold nanoparticles, GO possess a large accessible surface area and is a more effective superquencher (Huang and Liu, 2012) that can quench the fluorescence of various excited dyes through the photo-induced electron transfer (Chen et al., 2010; Piao et al., 2011) or long-range energy transfer (He et al., 2010; Zhao et al., 2011). More recently, conventional organic dye

* Corresponding author.
E-mail address: liuar@seu.edu.cn (A. Liu).
[1] These authors contributed equally to this work.

http://dx.doi.org/10.1016/j.bios.2016.11.070
Received 23 September 2016; Received in revised form 30 November 2016; Accepted 30 November 2016
Available online 01 December 2016
0956-5663/

molecules were replaced by highly bright quantum dots (QDs) for improving the signal-to-noise ratio (S/N) of such DNA probes, since compared with traditional organic dyes, the photoluminescence (PL) of QDs possesses a variety of advantages (Dong et al., 2010; He et al., 2010). However, almost all these detections are applied in aptamers (DNA) sensing, graphene based fluorescent detection was hardly used in immunoassay. The major factor limit the development of graphene-QD system is the strong fluorescence quenching effect caused by nonspecific adsorption which reduces the signal-to-noise ratio (S/N) of antibody probes. In DNA based fluorescent sensors, GO and the double stranded DNA (dsDNA) are all negatively charged, the electrostatic repulsion force would prevent them from nonspecific adsorption in a certain degree (Jang et al., 2010). Different from the DNA, the background caused by antigen or antibody are extremely exaggerated and intolerable, and so far, hardly any strategy has been reported solving the problem. Applying the antigen-antibody with GO-QDs to a fluorescent system would greatly expand the application field of the fluorescence detection, which is full of meaning, correspondingly it is a tremendous challenge and deserve us to explore and investigate.

Nanobodies (Nbs), also termed as Variable domains of heavy-chain antibodies (VHH) (Wang, et al., 2015a,b), is a unique type of conventional antibody fragment and naturally in the serum of camelidae. It is the smallest known antigen-binding antibody fragment (~15 kD) (Wang et al., 2015a,b), and has aroused a progressively attention in immunosensor for higher binding specificity and greater thermal stability (Cabanas-Danes et al., 2014; Ma et al., 2014), with hydrophilic residue substitutions in the framework-two region, it demonstrates a more soluble ability and a lower tendency for aggregation than conventional antibody (He et al., 2014). With these benefits, Nbs are more suitable than normal antibodies in the next fluorescent competitive immunosensors.

Herein, we developed a new graphene based fluorescent immunoassay and carry out an actual inspection by detection of CP4-EPSPS, as depicted in Scheme 1a. We fabricated two dimensional Graphene oxide/Polyacrylamide (GO/PAM) nanocomposites since the hydrophilic polymer chains on graphene could prevent nonspecific protein adsorption (Lin et al., 2014; Yang et al., 2015a, 2015b). High loading capacity and strong quenching effect of the carrier were obtained via an easy one-pot reaction. PAM was converted to Polyacrylic hydrazide (PAH), and thus more Nbs could be immobilized on polymer chains by amide bond. The quenching efficiency of GO was improved because after the restoration of the sp^2 crystal structure, the electronic transference ability of RGO certainly be promoted, which is beneficial to the fluorescence quenching (Lu et al., 2010.), and it was further strengthened via introducing the iron-containing particles to form a 2D Fe@RGO/PAH nanocomposites. By comparison, the biosensors constructed with Fe@RGO/PAH nanocomposites demonstrated a low signal loss caused by nonspecific adsorption, and the high quenching ability yield a nearly 4 fold signal intensity than unmodified GO. Subsequently, we fabricated the Fe@RGO/PAH/Nbs capture probes, the target Antigen (Ag) compete with the Ag/CdTe QDs@PEG, and the fluorescence signal intensity should gradually increase with increasing Ag concentration added.

2. Experimental section

2.1. Materials and methods

Details about materials, reagents, apparatus, characterization instruments, synthesis of Polyacryamide modified GO nanocomposites (GO/PAM), formation of Iron doped Polyacrylic Hydrazide modified RGO nanocomposites (Fe@RGO/PAH), construction of the immunofluorescence biosensor, determination of the CP4-EPSPS with the competitive immunofluorescent sensor and real-sample analysis are described in detail in the Supporting information.

3. Results and discussion

3.1. Characterization of 2D Fe@RGO/PAH nanocomposites

GO was synthesized by using modified Hummers' method (Yang et al., 2015a, 2015b.). AFM image showed that the as-prepared GO sheet has a single-layer atom structure with a thickness of about 1.2 nm on mica matrix (Fig. 1A), which is consistent with the early reports (Lei et al., 2011; Xu et al., 2008). After grafting with a hydrophilic molecular polyacrylamide (PAM) onto GO backbone through in-situ Free-Radical-Polymerization (FRP) (the equation shown in Fig. S2A), the AFM image of the polyacrylamide-grafted GO nanocomposites showed various protuberances growing on the sheet backbones with the average height of 3.5 nm, indicating the successful polymer grafting (Fig. 1B). The polymer chains were directly attached to the sp^2-hybridized or C-C double bonds of GO, rather than their functional groups. TEM image showed that the pristine GO sheets have a high transparent, clean and smooth surface (Fig. 1C), while the GO/PAM displayed numbers of polymer protuberances uniformly dispersing on the whole sheet that lead to an opaque GO backbone (Fig. 1D).

To improve the protein immobilization, the amide group of PAM on GO backbone was converted to hydrazide group by chemical reduction with hydrazine hydrate as reductant and $Fe(NO_3)_3{\cdot}9H_2O$ as catalyst (the equation shown in Fig. S2B). During the transamidation reaction with polyacrylamide and hydrazine, GO was reduced to reduced graphene oxide (RGO) simultaneously, while the Fe@RGO/PAH nanocomposites were loaded with iron containing nanoparticles. The conversion from GO to RGO can be illustrated by Raman spectra. Two prominent peaks at 1605 and 1328 cm^{-1} corresponding to the well documented G and D bands were clearly observed in the Raman spectrum of GO sheets (Fig. 2A). The similar D/G ratio of GO and GO/PAM indicated that the FRP reaction between the GO and acrylic amide do not cause obvious destruction of honeycomb lattice and sp^2 carbon network of graphene (Zhang et al., 2011a, 2011b). After reduction of GO/PAM with hydrazine, the band D/G ratio increased from 1.07 for GO/PAM to 1.49 for Fe@RGO/PAH, confirming the successful reduction of GO (Li et al., 2015).

The successful synthesis of Fe@RGO/PAH was demonstrated by X-ray photoelectron spectroscopy (XPS). Compared to GO sample, XPS analysis revealed that the peak of N_{1s} was clearly observed in GO/PAM sample (Fig. 2B). Elemental analysis showed a clear increase of N content for GO/PAM, indicating the successful FRP reaction (Table S1). C_{1s} high resolution XPS spectra of GO, GO/PAM and Fe@RGO/PAH were shown in Fig. 2C. Compared with GO, the C3 peaks (C–O bond, 286.7 eV) (Xu et al., 2009) of GO/PAM at high binding energy decreased due to the deoxygenation of GO by reduction, which was consistent with the XPS elemental quantification of oxygen, indicated the effective recovery of the π–system in GO (Stankovich et al., 2006.). Some asymmetry of the C_{1s} peak (deconvoluted as C2, C3, C4 and C5) were observed in Fe@RGO/PAH, primarily ascribed to the existence of C–N, C–O, C=O and –O–C=O (Chien et al., 2012). On one hand, it is difficulty in complete removal of the oxygen-defects, even with strong reduction reagents like hydrazine (Zhang et al., 2012). The other hand is the specific chemical bond (such as C–N) exist in PAM or PAH. Combining together with N_{1s} high resolution spectra (Fig. 2D), the main N1 peak with binding energy at 399.9 eV, revealed the existence of NH–C=O (Rodrigues et al., 2001) or NH–NH–C=O (Liu et al., 2007). The N2 peak in 401.5 eV represented the C–N–H, such as NH_2 (Zhou et al., 2015.). It should be noted that the signal of N–H bond which should have been in 400.2 eV (Sadough Vanini., Audouard and Marcus, 1994) was too close with N1 to distinguish, overlapped by the amide bond. All these results confirmed the successful grafting of PAM onto GO and conversion from GO to RGO accompanying with the transamidation reaction. The formation of hydrazide can be further confirmed by an indirectly UV–*vis* spectroscopy measurements based on the formation of chromogenic product of hydrazone derivative through

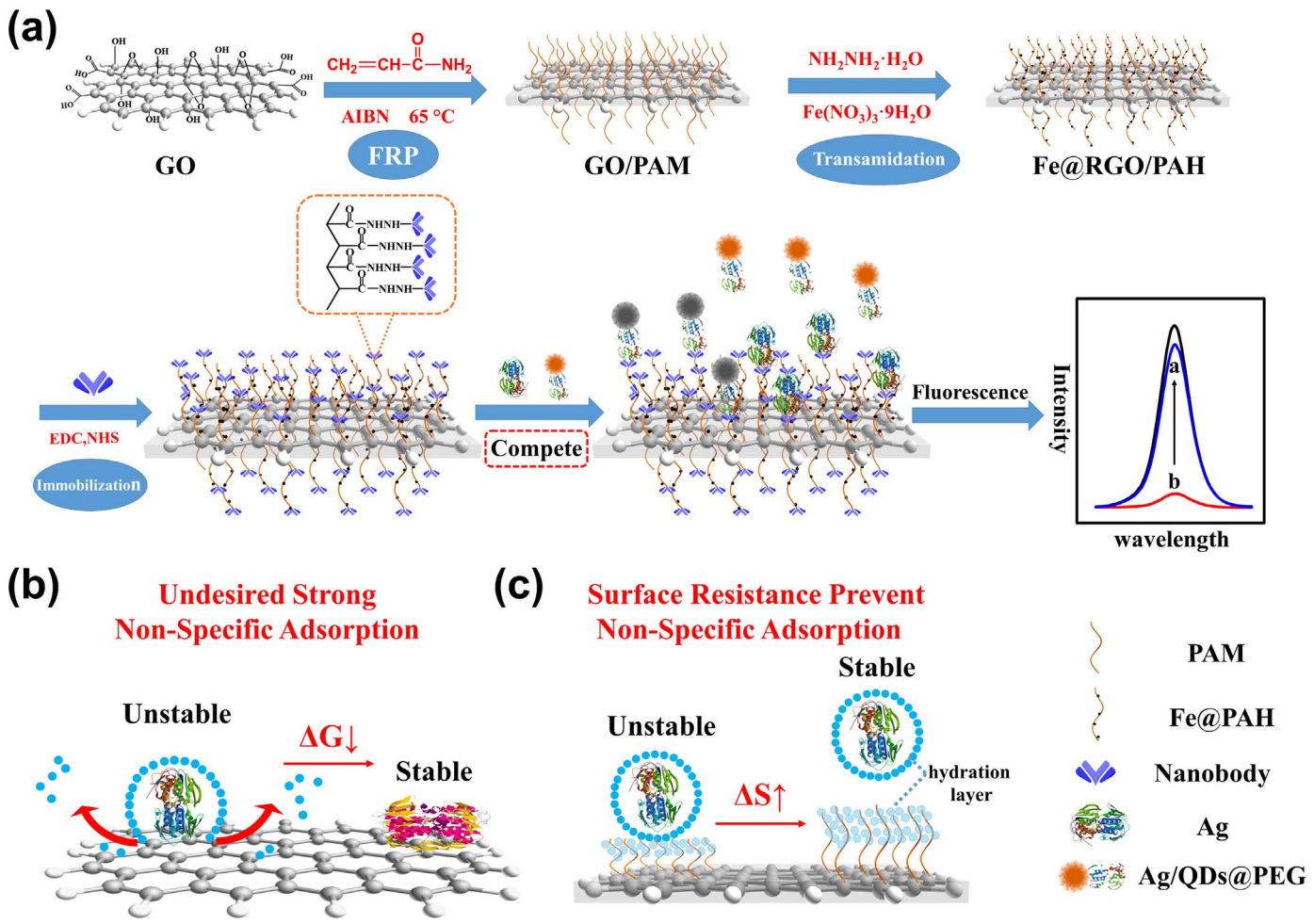

Scheme 1. (a) Construction process of the fluorescent competitive immunosensors with the 2D Fe@RGO/PAH Nanocomposites. Mechanism of (b) strong nonspecific adsorption and (c) anti-adsorption between antigen and carrier materials.

the reaction between hydrazide and *p*-nitrobenzaldehyde. (Greg, 2008.). After reacting with *p*-nitrobenzaldehyde, the Fe@RGO/PAH nanocomposites displayed a new absorption at 323 nm, which belonged to the hydrazone derivative formed by Schiff base interaction of aldehyde and hydrazide(Fig. S3), confirming the successful transformation from PAM to PAH.

$Fe(NO_3)_3$ was hydrolyzed in alkaline solution during the transamidation reaction, thus iron containing nanoparticles with the size of several nanometers were formed and dispersed homogenously on the graphene sheets (TEM, Fig. 2E), considering the element analysis (iron content 2.98%). In Fig. 2B, The X-ray photoelectron spectroscopy (XPS) was used to investigate the electronic structure of iron containing particles on the Fe@RGO/PAH nanocomposites. The XPS Fe 2p core level spectra show the peak position at 711.5 eV for the Fe-O bond (Serov et al., 2014.). Ferric oxide nanoparticles were formed as the result of $Fe(NO_3)_3$ hydrolysis. The surface of ferric oxide nanoparticles was commonly positive charged, which can be loaded onto graphene nanocomposite via electrostatic interaction. As shown in Fig. S4, the Zeta potential of GO is negative (−30.5 mV) and the Zeta potential of Fe@RGO/PAH increased to (−22.5 mV), owing to the loading of the incorporation of iron containing nanoparticls. The EDX elemental mapping of Fe@RGO/PAH (Fig. 2F) clearly observed the homogeneous distribution of the Fe element in the whole carbon framework.

3.2. Competitive immunofluorescence sensing strategy

Nbs were coupled to Fe@RGO/PAH nanocomposites through the carbodiimide-mediated amidation reaction between hydrazide and the carboxyl in Nbs with the help of EDC and NHS. The circular dichroism (CD) spectra of Fe@RGO/PAH/Nbs showed a couple of well-define peaks in 217 nm (Fig. 3A), which is the same as the CD behavior of Nbs free in solution specifically caused by the β fold of protein (Zhu et al., 2015). While no CD signal was observed on GO and Fe@RGO/PAH, indicating that the Nbs were immobilized on the 2D Fe@RGO/PAH successfully.

The as-prepared Fe@RGO/PAH/Nbs played the role as both nanobodies' carrier and fluorescence quencher. Fluorescence emission spectra of the Ag/QDs@PEG before and after adding GO or Fe@RGO/PAH nanocomposites with or without Nbs coupling as quenchers was shown in Fig. 3B. The fluorescence intensity of Ag/QDs@PEG reduced to 46.47% or 27.75% of its original intensity after adding 0.5 μg/mL GO or 0.5 μg/mL Nbs/GO into 100 ng/mL Ag/QDs@PEG solution. Such high background could be explained by the strong, inevitable nonspecific adsorption between GO and protein (Scheme 1b). Once the protein contact to the hydrophobic surface of GO, The surface-protein contact area induces a gain in free energy and hence proteins tend to maximize their footprint through a conformational re-organization (Rabe et al., 2011.), forming a "hydrophilic portion inward, outward hydrophobic portion" conformation, which cause the aggregation or clustering of proteins, subsequently spread out on large, hydrophobic surface of GO and tightly combined (Rabe et al., 2011.). As a contrast, the fluorescence intensity reduced to 69.27% of the original intensity after 0.5 μg/mL of Fe@RGO/PAH nanocomposites were added into Ag/QDs@PEG solution as quencher, indicating the low fluorescence quenching effect caused by nonspecific adsorption. Therefore, the formation of polymer chains on graphene was able to resist nonspecific

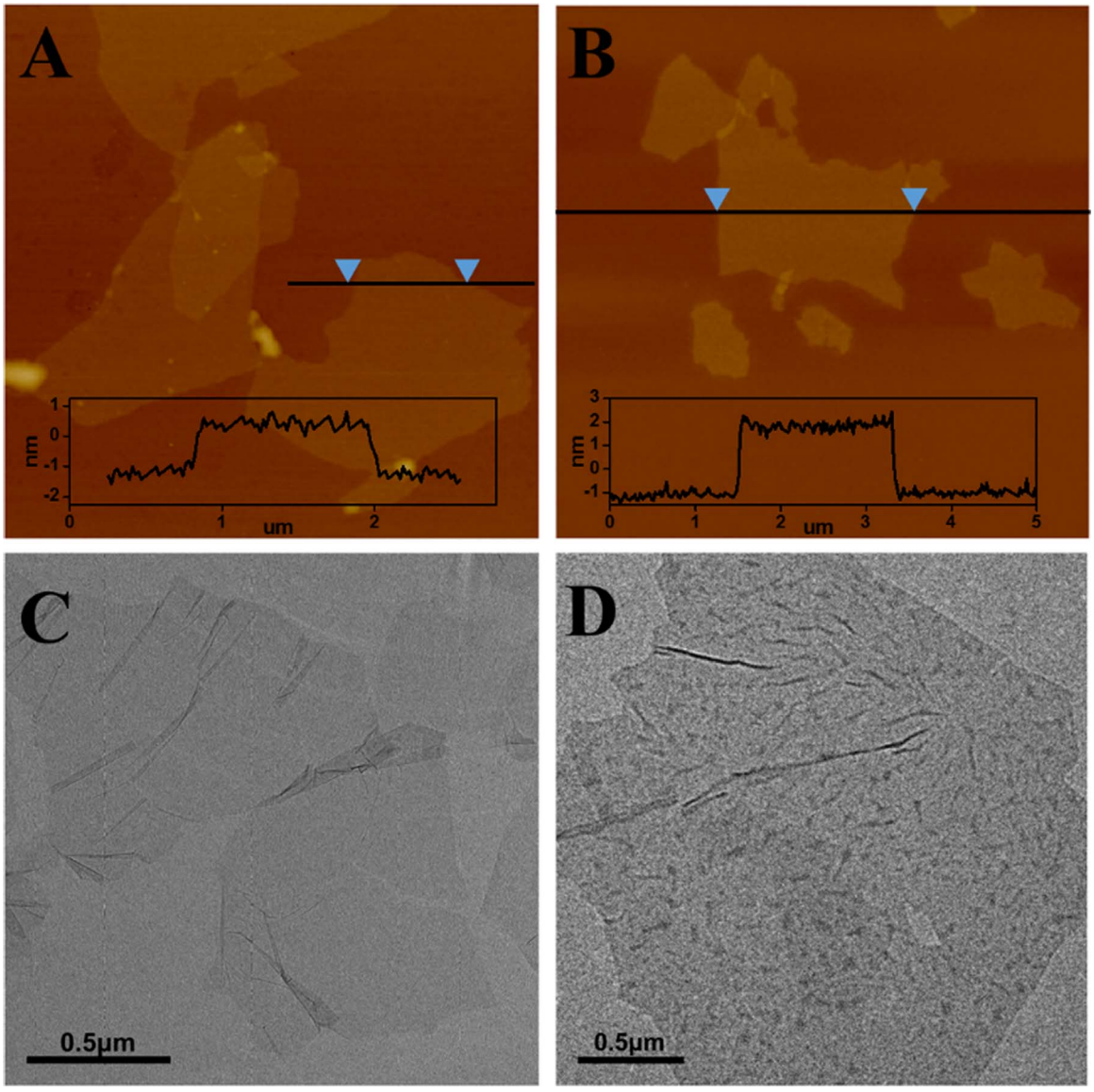

Fig. 1. AFM height images of (A) GO and (B) GO/PAM (size for AFM images: 5 μm×5 μm). Corresponding TEM images of (C) GO and (D) GO/PAM.

protein adsorption. When 0.5 μg/mL Fe@RGO/PAH/Nbs were added to Ag/QDs@PEG solutions as the quencher instead, the fluorescence intensity reduced rapidly to 6.33% of the original intensity, indicating the strong quenching effect of Fe@RGO/PAH/Nbs on the fluorescence of QDs. The low fluorescence quenching effect caused by nonspecific absorption of Fe@RGO/PAH nanocomposites can be explained by three reasons and displayed in Scheme 1c. Firstly, both Fe@RGO/PAH and Ag/QDs@PEG were hydrophilic and negatively charged (zeta potential shown in Fig. S4), and the electrostatic repulsion force prevented them from contacting. Secondly, the nonfouling ability of RGO/PAH cause a hydration layer near the carrier surface because a tightly bound water layer associated with PAH chains by hydrogen-bond forms a physical and energetic barrier to avoid protein adsorption on the surface of Fe@RGO/PAH, which called the “water barrier” (Nagasawa et al., 2015; Penna et al., 2014.). Finally, the “steric repulsion” theory is also an important key point (Feng et al., 2011; Inoue et al., 2013.). When protein approaches to the surface of PAH, the compression of the polymer chains cause steric repulsion to resist protein adsorption due to unfavorable decrease in entropy. Moreover the fluorescence quenching caused by the nonspecific adsorption can be further decreased by reducing the usage amount of Fe@RGO/PAH nanocomposites as optimization (shown in the part of optimization experiment and Fig. 4B).

The fluorescence of excited QDs was quenched possibly through the photo-induced electron transfer from QDs to GO based materials (Chen et al., 2010; Piao et al., 2011.). The high quenching ability of Fe@RGO/PAH/Nbs is mainly ascribed to two factors. On one hand is excellent quenching performance of the carrier materials. As shown in Fig. S5A, after reduction of GO, the fluorescence quenching effect was little increased but lower than that of Fe@RGO/PAH/Nbs. The improved quenching ability of Fe@RGO/PAH may be influenced by the reduction of GO and the incorporation of iron containing nanoparticls. A possible reason is that the electronic transference rate of the material was increased (Liu et al., 2016). Finally, the high quenching ability of Fe@RGO/PAH yield a nearly 4 fold signal intensity than unmodified GO in same condition (Fig. S5B). The fluorescence lifetime of the Ag/QDs, Ag/QDs+GO/Nbs and Ag/QDs+Fe@RGO/PAH/Nbs was investigated. As shown in Fig. S6, the fluorescence lifetime of Ag/QDs is 13.14 ns. After quenched by GO/Nbs, the fluorescence life time changed to 10.22 ns. After quenched by Fe@RGO/PAH/Nbs, the fluorescence life time decreased to 5.02 ns. This result indicated that the improved fluorescence quenching effects of Fe@RGO/PAH/Nbs was partially owing to the faster electronic transference of the nanocomposites. On the other hand, the protein conformation of normal antibodies (Abs)

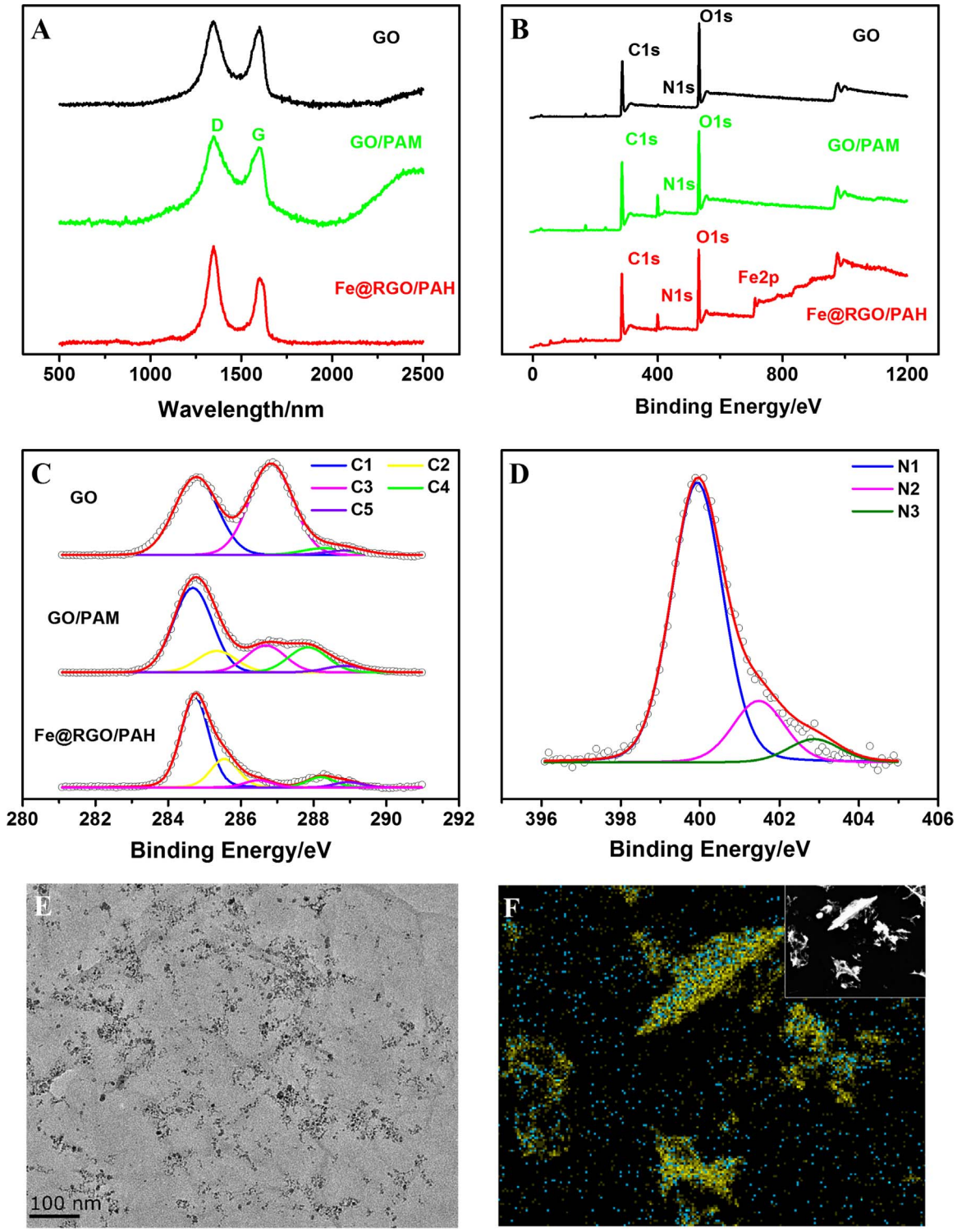

Fig. 2. (A) Raman spectra, (B) XPS survey spectra and (C) high resolution C_{1s} spectra of GO, GO/PAM and Fe@RGO/PAH Nanocomposites. (D) XPS N_{1s} high resolution spectra and (E) TEM image of Fe@RGO/PAH Nanocomposites. (F) EDX elemental mapping merge graph of Fe@RGO/PAH Nanocomposites, where the blue and yellow points represent N and Fe atom respectively, the inset was the corresponding Bright field (BF) SEM image.

would be re-organized when they were coupled to the hydrophobic basal plane of graphene. It may affect the immunoreaction between Abs and Ag/QDs@PEG, and therefore only a little amount of Ag/QDs@PEG being coated onto GO/Abs surface, which led the quenching efficient lowed slightly. As contract, the hydrophilic surface of Fe@RGO/PAH and the high stable ability of Nbs would not cause the conformational re-organization of Nbs, and the native conformation is in favor of the recognition between the Nbs and Ag, which made the quenching more effectively.

The high quenching ability of Fe@RGO/PAH/Nbs can be used for detection of CP4–EPSPS based on competitive immunoassay. The free antigen CP4–EPSPS possessed stronger specific binding ability with the Nbs than the labeled antigen (Ag/QDs@PEG). When the free antigen was mixed with Fe@RGO/PAH/Nbs and the labeled antigen, less labeled antigen would bind with the Nbs on Fe@RGO/PAH and the fluorescent quenching caused by the specific binding between Nbs

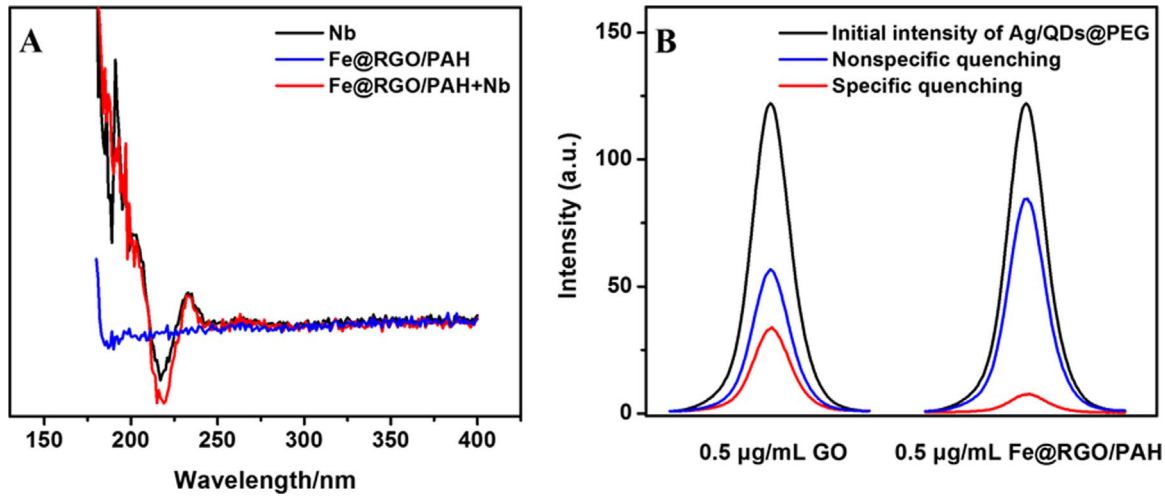

Fig. 3. (A) Circular Dichroism (CD) spectra of Fe@RGO/PAH/Nbs probe. (B) Fluorescence emission spectra of the Ag/QDs@PEG under different conditions: Ag/QDs@PEG (black curve); Ag/QDs@PEG +0.5 μg/mL GO or Ag/QDs@PEG +0.5 μg/mL Fe@RGO/PAH (blue curve); Ag/QDs@PEG +0.5 μg/mL GO/Nbs or Ag/QDs@PEG +0.5 μg/mL Fe@RGO/PAH/Nbs (red curve).

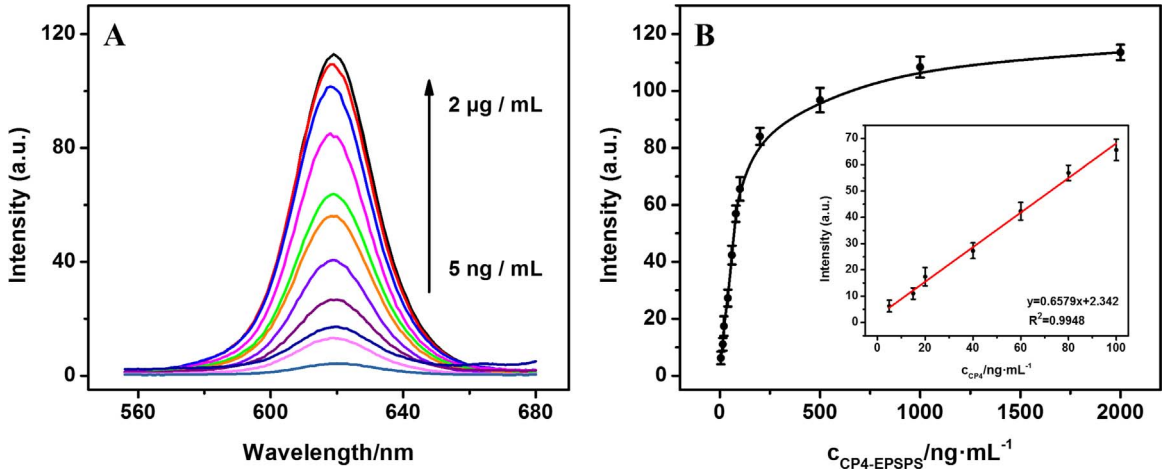

Fig. 4. (A) Fluorescence emission spectra and (B) plot of fluorescent intensity of 30 ng/mL Nbs/Fe@RGO/PAH mixture solution containing 100 ng/mL Ag/QDs@PEG and different concentrations of Ag from 5 ng/mL to 2 μg/mL. The inset in B shows linear response at low Ag concentrations from 5 to 100 ng/mL.

and the labeled antigen would be decreased. In this case, a certain amount of Ag/QDs@PEG (100 ng/mL) and a series of concentrations of CP4–EPSPS, eg., 5.0 ng-2.0 μg/mL, were mixed uniformly and added to Fe@RGO/PAH/Nbs solution. The immunoreaction was allowed to react for 20 min, the fluorescence of the resulting mixture was then detected. With the increasing concentration of CP4–EPSPS, more free target Ag would combine with the Nbs on Fe@RGO/PAH, which decreased the fluorescent quenching efficiency due to less Ag/QDs@PEG bound to Fe@RGO/PAH. Based on this competitive immunosensing strategy, a quantitative fluorescent method was developed for CP4–EPSPS detection.

3.3. Optimization of the immunoassay conditions

The performance of competitive immunoassay usually depends on the reaction time between the Nbs and antigen, the usage amount of the Fe@RGO/PAH and Nbs. The conditions above were all optimized to get the maximum signal to noise ratio, and thus obtain lower LOD and wider detection range.

As shown in Fig. S7A, by addition of Fe@RGO/PAH/Nbs into the mixture solution of free Ag and Ag/QDs@PEG, the quenching efficiency enhanced largely with the incubation time at the first 13 min, then it was quenched slowly and completely at 20 min. Therefore, 20 min was employed as the optimum time for the incubation between Fe@RGO/PAH/Nbs and the mixture solution of free Ag and Ag/QDs@PEG.

When the amount of Ag/QDs@PEG was fixed to 100 ng/mL, the usage amount of the Fe@RGO/PAH/Nbs was a critical factor to the sensing. As shown in Fig. S7B, too little Fe@RGO/PAH was inadequate to a desired quenching effect, and with the incensement of Fe@RGO/PAH, the quenching effect was improved correspondingly. When the concentration was 30 ng/mL, the desired quenching was about 92% and nonspecific quenching was 10%. When the concentration was further increased, although more Fe@RGO/PAH can create an almost 100% quenching effect, the excessive use made a higher nonspecific quenching, which decreased the intensity and accuracy of the detection. As a result, 30 ng/mL was chosen as the best value for use.

Furthermore, the amount of Nbs immobilized on the Fe@RGO/PAH was optimized shown in Fig. S7C. When the amount of Nbs was low, the Ag/QDs@PEG in solution was unable to be captured to Fe@RGO/PAH/Nbs, as a result, low quenching efficient and large background was obtained. When Nbs were more than 50 ng/mL, the fluorescence quenched completely. Since further increase of capture probe numbers was adverse to LOD in competitive method, therefore, the concentration of Nbs was optimized to be 50 ng/mL.

Table 1
Recovery Results of CP4-EPSPS Added in Real Samples.

Sample no.	Added (ng/mL)	Found (ng/mL)	Recovery (%)	RSD (%,n=5)
1	0	–	–	–
2	3	2.89	96.20	7.55
3	10	10.60	105.95	3.13
4	30	30.90	103.01	2.20
5	50	46.02	92.05	3.65
6	100	95.77	95.77	2.58

3.4. Determination of CP4–EPSPS and real samples analysis

Upon the optimum conditions, the fluorescence intensity varied with different concentration of target Ag (Fig. 4A), and it can be found that fluorescent intensity value displays a well linearly proportional to concentration of target in the range from 5 to 100 ng/mL.(Fig. 4B), the regression equation was y=0.6579x+2.342, with the correlation coefficient of 0.9948. The limit of detection is 0.34 ng/mL (LOD, S/N=3), which was much lower than the reported ELISA (94 ng/mL) (Jennings et al., 2003.), LC–MS/MS (47 ng/mL) (Zhang et al., 2014.) or other method.

Finally, a significant and challenging factor for CP4-EPSPS analysis is the applicability in actual biological matrixes. So far no standard methods have been reported for the quantitative detection of CP4–EPSPS in GM crops and the content of CP4–EPSPS in GM crops cannot be estimated accurately for comparison. Thus, a standard addition method was applied in real sample analysis with the proposed immunofluorescent biosensor. As dry or wet heating could cause protein denaturation in the real samples, non-GMO corn leaf extraction was used in the analog experiment. The prepared homogenate from non-GMO corn leaves was centrifuged at 6000 rpm for 30 min and the supernatant was collected.100 μL supernatant was spiked with 3, 10, 30, 50, and 100 ng target Ag respectively and were analyzed by using the proposed method. Results were shown in Table 1 and exhibited good recoveries varied in the range of 92.05–105.95%. The relative standard derivations (RSD) were from 2.16% to 7.55%, indicating our method had high precision and good reliability for detection of CP4-EPSPS in real examinations. Therefore, the results demonstrated that the proposed method could be further used for quantification of CP4-EPSPS in complex real sample extractions.

3.5. Stability, Reproducibility and Specificity

Storage stability of the proposed immunosensor was investigated by storing the same Fe@RGO/PAH/Nbs homogenous solution at 4 °C under darkness for different periods before the fluorescence detection of 10 ng/mL CP4–EPSPS. It was clear that 90.75% of the quenching effects (Fig. S8) for the immunosensor was retained after storage for 4 weeks, indicating that the prepared immunosensor possesses good stability and potential for practical application. The stability of the immunoassay can be explained as follows: In our immunoassay, attribute to hydrophilic polymer grafted to RGO, the π-π stacking between graphene was avoided. Fe@RGO/PAH and Ag/QDs@PEG repelled with each other, not only keeping a well dispersion of graphene, but also improving the accuracy of detection by decreasing the uncertainty of random contact between the Fe@RGO/PAH and Ag/QDs@PEG. In addition, the well biological compatibility of RGO and excellent thermal stability of Nbs also contribute to establish a stable system.

Attributed to the stable system, a good accuracy and reproducibility were also obtained (Table S2). Various concentrations of standard CP4-EPSPS was detected five times respectively with the proposed method (in the way of intra-assay and interassay), the intra-assay variability (CV %=SD/mean) of 4.16% and the interassay variability of 6.62% both suggest a good reproducibility of the proposed immunosensor.

The specificity of the proposed immunosensor was investigated by measuring the sensor responses to HCG, PSA, AFP, NDKA and Bt at a concentration of 100 ng/mL that is 10 fold to CP4–EPSPS, shown in Fig. S9. The fluorescence intensity of the interfering antigens was much lower than that of CP4–EPSPS. Since all the interfering antigens could not specifically bind to the Fe@RGO/PAH/Nbs probe, almost all the QD-labeled CP4-EPSPS antigen bound to the Fe@RGO/PAH/Nbs probe and then be quenched. A significant fluorescence increase was observed for their mixture with CP4–EPSPS, indicating that intensity of sensors was mainly caused by a specific antibody–antigen immunoreaction. The influence of metal ions and acid radical ions during the fluorescent detection was also investigated. As shown in Fig. S10A, the Fe@RGO/PAH/Nbs probe remained high quenching efficiency in the solution of 0.01 mol/L Na^+, K^+, Ca^{2+}, Mn^{2+}, Zn^{2+} and the mixed solution. As shown in Fig. S10B, the Fe@RGO/PAH/Nbs probe also remained high quenching efficiency in the solution of 0.01 mol/L Cl^-, NO_3^-, SO_4^{2-}, $HPO_4^{2-}/H_2PO_4^-$, CH_3COO^- and the mixed solution. The result indicated that the Fe@RGO/PAH/Nbs probe had strong resistance to interference of metal ions and acid radical ions.

4. Conclusion

This work proposed a simple but ultrasensitive competitive immunosensors for accuracy quantitative detection of CP4–EPSPS based on a novel antibody VHH (Nanobody). The key problem of the platform is the inevitable but strong nonspecific interaction between the target and GO, and it was solved by synthesizing a hydrophilic GO polymer brushers. It was further consummated via a simple but effective one pot reaction to improve the fluorescence quenching efficiency and increase the loading capacity of nanobodys at the same time. The final formed Fe@RGO/PAH nanocomposites accelerated the electron transfer rate, reduced the background noise and greatly enhanced the detection signal. The LOD of the proposed sensors for CP4-EPSPS detection was 0.34 ng/mL, which is much lower than the existed method. This designed sensing strategy not only served as universal tool that can be expanded to detect different target biomarker including but not just protein, but also provide a powerful tool for investigation of fluorescent sensing processes with numerous multifunctional GO based materials.

Notes

The authors declare no competing financial interest.

Acknowledgements

This work was financially supported by the National Natural Science Foundation of China (21505018), the Natural Science Foundation of Jiangsu Province of China (BK 20141348) and Fundamental Research Funds for the Central Universities.

Appendix A. Supporting information

Supplementary data associated with this article can be found in the online version at doi:10.1016/j.bios.2016.11.070.

References

Ahmed, F.E., 2002. Trends Biotechnol. 20, 215–223.
Cabanas-Danes, J., Rodrigues, E.D., Landman, E., van Weerd, J., van Blitterswijk, C., Verrips, T., Huskens, J., Karperien, M., Jonkheijm, P., 2014. J. Am. Chem. Soc. 136, 12675–12681.
Chang, H.X., Tang, L.H., Wang, Y., Jiang, J.H., Li, J.H., 2010. Anal. Chem. 82, 2341–2346.
Chang, P.-C., Reddy, P.M., Ho, Y.-P., 2014. Anal. BioAnal. Chem. 406, 5339–5346.
Chen, Z.Y., Berciaud, S., Nuckolls, C., Heinz, T.F., Brus, L.E., 2010. ACS Nano 4, 2964–2968.
Chien, C.T., Li, S.S., Lai, W.J., Yeh, Y.C., Chen, H.A., Chen, I.S., Chen, L.C., Chen, K.H.,

Nemoto, T., Isoda, S., Chen, M., Fujita, T., Eda, G., Yamaguchi, H., Chhowalla, M., Chen, C.W., 2012. Angew. Chem. Int. Ed. 51, 6662–6666.
Dong, H.F., Gao, W.C., Yan, F., Ji, H.X., Ju, H.X., 2010. Anal. Chem. 82, 5511–5517.
Feng, W., Gao, X., McClung, G., Zhu, S.P., Ishihara, K., Brash, J.L., 2011. Acta Biomater. 7, 3692–3699.
Hermanson, Greg T., 2008. Bioconjugate Techniques (2nd ed). Elsevier, Rockford.
He, S.J., Song, B., Li, D., Zhu, C.F., Qi, W.P., Wen, Y.Q., Wang, L.H., Song, S.P., Fang, H.P., Fan, C.H., 2010. Adv. Funct. Mater. 20, 453–459.
He, T., Wang, Y.R., Li, P.W., Zhang, Q., Lei, J.W., Zhang, Z.W., Ding, X.X., Zhou, H.Y., Zhang, W., 2014. Anal. Chem. 86, 8873–8880.
Huang, P.J.J., Liu, J.W., 2012. Anal. Chem. 84, 4192–4198.
Inoue, Y., Nakanishi, T., Ishihara, K., 2013. Langmuir 29, 10752–10758.
Jang, H.J., Kim, Y.K., Kwon, H.M., Yeo, W.S., Kim, D.E., Min, D.H., 2010. Angew. Chem. Int. Ed. 49, 5703–5707.
Jennings, J.C., Kolwyck, D.C., Kays, S.B., Whetsell, A.J., Surber, J.B., Cromwell, G.L., Lirette, R.P., Glenn, K.C., 2003. J. Anim. Sci. 81, 1447–1455.
Lei, Y.D., Tang, Z.H., Liao, R.J., Guo, B.C., 2011. Green Chem. 13, 1655–1658.
Lerat, S., Gulden, R.H., Hart, M.M., Powell, J.R., England, L.S., Pauls, K.P., Swanton, C.J., Klironomos, J.N., Trevors, J.T., 2007. J. Agr. Food Chem. 55, 10226–10231.
Li, Y.Y., Lu, Q.H., Liu, H.L., Wang, J.F., Zhang, P.C., Liang, H.G., Jiang, L., Wang, S.T., 2015. Adv. Mater. 27, 6848–6854.
Lin, J.H., Chang, H.Y., Kao, W.L., Lin, K.Y., Liao, H.Y., You, Y.W., Kuo, Y.T., Kuo, D.Y., Chu, K.J., Chu, Y.H., Shyue, J.J., 2014. Langmuir 30, 10328–10335.
Liu, L., Lang, J.W., Zhang, P., Hu, B., Yan, X.B., 2016. ACS Appl. Mater. Interfaces 8, 9335–9344.
Liu, X.Y., Chen, S.H., Zhai, H.Y., Shen, L.X., Zhou, J.J., Wu, L., 2007. Electrochem. Commun. 9, 813–819.
Lu, C.H., Li, J., Lin, M.H., Wang, Y.W., Yang, H.H., Chen, X., Chen, G.N., 2010. Angew. Chem. Int. Ed. 49, 8454–8457.
Lu, C.H., Yang, H.H., Zhu, C.L., Chen, X., Chen, G.N., 2009. Angew. Chem. Int. Ed. 48, 4785–4787.
Ma, L., Sun, Y.Y., Kang, X.J., Wan, Y.K., 2014. Biosens. Bioelectron. 61, 165–171.
Marani, M.M., Costa, J., Mafra, I., Oliveira, M.B., Camperi, S.A., Leite, J.R., 2015. Biopolymers 104, 91–100.
Nagasawa, D., Azuma, T., Noguchi, H., Uosaki, K., Takai, M., 2015. J. Phys. Chem. C 119, 17193–17201.
Ocana, M.F., Fraser, P.D., Patel, R.K., Halket, J.M., Bramley, P.M., 2009. Anal. Chim. Acta 634, 75–82.
Penna, M.J., Mijajlovic, M., Biggs, M.J., 2014. J. Am. Chem. Soc. 136, 5323–5331.
Piao, Y.X., Liu, F., Seo, T.S., 2011. Chem. Commun. 47, 12149–12151.
Rabe, M., Verdes, D., Seeger, S., 2011. Adv. Colloid Interfac. Sci. 162, 87–106.
Rodrigues, P.C., Muraro, M., Garcia, C.M., Souza, G.P., Abbate, M., Schreiner, W.H., Gomes, M.A.B., 2001. Eur. Polym. J. 37, 2217–2223.
Sadough Vanini, A., Audouard, J.P., Marcus, P., 1994. Corros. Sci. 36, 1825–1834.
Serov, A., Artyushkova, K., Atanassov, P., 2014. Adv. Energy Mater. 4, 1301735(1–7).
Singh, M., Randhawa, G.J., Sood, P., Bhoge, R.K., 2015. Food Control. 51, 283–292.
Stankovich, S., Piner, R.D., Chen, X.Q., Wu, N.Q., Nguyen, S.T., Ruoff, R.S., 2006. J. Mater. Chem. 16, 155–158.
Swope, N.K., Fryfogle, P.J., Sivy, T.L., 2015. J. Chem. Educ. 92, 1229–1232.
Wang, H., Li, G.H., Zhang, Y.H., Zhu, M., Ma, H.M., Du, B., Wei, Q., Wan, Y.K., 2015. Anal. Chem. 87, 11209–11214.
Wang, J., Majkova, Z., Bever, C.R., Yang, J., Gee, S.J., Li, J., Xu, T., Hammock, B.D., 2015. Anal. Chem. 87, 4741–4748.
Xu, Y.X., Bai, H., Lu, G.W., Li, C., Shi, G.Q., 2008. J. Am. Chem. Soc. 130, 5856–5857.
Xu, Y.X., Zhao, L., Bai, H., Hong, W.J., Li, C., Shi, G.Q., 2009. J. Am. Chem. Soc. 131, 13490–13497.
Yang, J., Hua, Z., Wang, T., Wu, B., Liu, G.M., Zhang, G.Z., 2015a. Langmuir 31, 6078–6084.
Yang, X.Q., Liu, A.R., Zhao, Y.W., Lu, H.J., Zhang, Y.J., Wei, W., Li, Y., Liu, S.Q., 2015b. ACS Appl. Mater. Interfaces 7, 23731–23740.
Zhang, M., Teng, Z.Q., Xu, W., Dai, R.J., Qing, H., Deng, Y.L., Xu, J.G., 2014. Anal. Methods 6, 7399–7406.
Zhang, S.P., Xiong, P., Yang, X.J., Wang, X., 2011a. Nanoscale 3, 2169–2174.
Zhang, Y.J., Fugane, K., Mori, T., Niu, L., Ye, J.H., 2012. J. Mater. Chem. 22, 6575.
Zhang, Y., Liu, Y., Zhen, S.J., Huang, C.Z., 2011b. Chem. Commun. 47, 11718–11720.
Zhao, X.H., Kong, R.M., Zhang, X.B., Meng, H.M., Liu, W.N., Tan, W., Shen, G.L., Yu, R.Q., 2011. Anal. Chem. 83, 5062–5066.
Zhou, Z.X., Shen, Y.F., Li, Y., Liu, A.R., Liu, S.Q., Zhang, Y.J., 2015. ACS Nano 9, 12480–12487.
Zhu, L.J., Song, Y., Cheng, P.N., Moore, J.S., 2015. J. Am. Chem. Soc. 137, 8062–8068.